

Phase transitional ferroelectric like behaviour of ammonium tetroxalate dihydrate single crystal

Eunice Jerusha^a & S Shahil Kirupavathy^{b*}

^aDepartment of Physics, R M D Engineering College, Kavariipettai 601 206, India

^bDepartment of Physics, Velammal Engineering College, Chennai 600 066, India

Received 21 February 2017; accepted 15 May 2018

Dielectric characterisation on ammonium tetroxalate dihydrate (ATOXAL) single crystal has been carried out. The dielectric constant and dielectric loss studied as a function of temperature and frequency have been found to have anomalous variations in the vicinity of the phase transitions at 100 °C and 140 °C which have been duly supported by thermal studies. An Arrhenius shift in the temperature variation of relaxation frequency has estimated the activation energy and the means of conduction. The ferroelectric and paraelectric phase activation energies have been determined to be 1.772 eV and 3.477 eV, respectively. The Penn band gap is 1.892 eV and the polarizability has been evaluated. The piezoelectric coefficient d_{33} has been found to be 1.5 pC/N⁻¹. The ferroelectric hysteresis behaviour has been investigated at room temperature. From the hysteresis loop it is found that the grown crystal exhibits a remanent polarization (P_r) \sim 0.367 μ C/cm², saturation polarisation (P_s) \sim 1.789 μ C/cm² and coercive field (E_c) \sim 6.599 kV/cm.

Keywords: Dielectric, Conductivity, Penn gap, Piezoelectric, Hysteresis

1 Introduction

Ferroelectric crystals are non-polar above the Curie temperature but are spontaneously polarized with a spontaneous lattice distortion below the Curie temperature. The interesting properties of ferroelectrics arise from the fact that it is possible to change the polarization and distortion through applied electric field or mechanical stress. Further, there is typically a reduction in crystallographic symmetry at the Curie temperature and this creates more than one symmetry-related, spontaneously polarized and distorted state below this temperature. The different states can coexist as domains in very intricate and characteristic domain patterns^{1,2}. These domains can be switched and the domain patterns are manipulated by the application of electric field and mechanical stress. Domain switching with its large change in polarization and lattice distortion provides a potent mechanism for obtaining large and unusual properties.

The physical properties of real ferroelectric crystals which are characterized to a great extent by the state and dynamics of domain structure, kinetics of phase transition, the interaction of domain walls, and phase boundaries with defects etc. can be investigated by a frequency – temperature varied dielectric spectroscopic method.

Characteristic phase transitions, resulting in dramatic changes in a variety of physical properties are seen in many crystalline ammonium compounds when their temperature is changed. Measurement of the electrical properties of such materials can also yield valuable information about the phase transitions. Ammonium tetroxalate dihydrate, (NH₄H₃(C₂O₄)₂·2H₂O (ATOXAL)), is a very interesting crystal belonging to the above category of materials. Previous investigations on this material include original determination of crystal structure by neutron diffraction³, EPR studies⁴, X-ray studies⁵ and anisotropic elastic properties⁶. Though the works were carried out earlier to understand the fundamental properties of ATOXAL, few of the basic characteristics were not probed. Hence attempts were made to study the various structural, mechanical, optical, thermal and morphological properties. The present work is in continuation of these various characterization studies which were meted out on the title material⁷ and the results of various dielectric, ferroelectric and piezoelectric characterization studies performed on the grown crystals are reported for the very first time.

2 Experimental Work

2.1 Crystal growth

Ammonium oxalate monohydrate (NH₄)₂C₂O₄·H₂O and oxalic acid dihydrate C₂O₄H₂·2H₂O were taken in

*Corresponding author (E-mail: shahilkirupavathy@yahoo.co.in)

an appropriate ratio and dissolved in deionised water, and the solution was heated slightly above room temperature. The solution was filtered after continual stirring for 6 h to remove any impurities. The filtered solution was housed in a constant temperature bath and optimally closed for controlled evaporation of the solvent. Colourless ATOXAL crystals measuring $13 \times 10 \times 4 \text{ mm}^3$ dimension were obtained over a 4 week growth period. The reaction mechanism is given in Scheme 1.

From the single crystal XRD data it is confirmed that ATOXAL crystallizes in the triclinic system with space group $P\bar{1}$ and $Z = 2$. The obtained crystallographic data are in good agreement with that reported in literature⁵ and are listed in Table 1.

2.2 Characterisation

The NETZSCH DSC 200F3 was used to study the phase transition that occurred in the ATOXAL crystal. The HIOKI 3532 – 50 LCR HITESTER was used to analyse the crystal sample for its dielectric behaviour. Good ohmic contact of the silver coated samples was established by cutting the crystal with a diamond saw and polishing using paraffin oil and fine grade alumina powder. The dielectric measurements were performed in the frequency range 50 Hz – 50 MHz and temperature range 40 °C – 160 °C using a two terminal sample holder at a heating rate of 5 °C/min. Automation was done for the temperature controller. Data recording, storage and analysis were performed using a computer. Piezoelectric coefficient d_{33} of the grown crystal was measured using Piezotest Piezometer PM-300 system. The P - E hysteresis loops for the ATOXAL crystals were traced at room temperature for a frequency of 50 Hz using an

automatic P - E loop tracer with a modified Sawyer Tower circuit. Thin polished samples painted with dry silver paste acted as electrodes.

3 Results and Discussion

3.1 Thermal analysis

The DSC curve presented in Fig. 1 shows the thermal anomalies observed at 95 °C and 170 °C. The first peak maybe attributed to the expansion of the material leading to the dissociation and dehydration of H_2O molecules along with the release of CO . A structural change is possible leading to a phase transition as is observed in the dielectric studies conducted on the crystal. ATOXAL can therefore be classified as a ferroelectric material. The second peak corresponds to the subsequent melting and decomposition of the crystal sample during which gases like CO_2 , NH_3 and H_2 are released. These observations correspond with TG/DTA measurements carried out on the sample.

3.2 Dielectric measurements

Results from literature^{8,9} make obvious the fact that even centrosymmetric crystals exhibit ferroelectricity. The reversal of centrosymmetric structure to a non-centrosymmetric one occurs under the influence of a very strong electric field due to the distortion in the local geometry of the centrosymmetric crystal. Thus, giving rise to ferroelectricity accompanied by

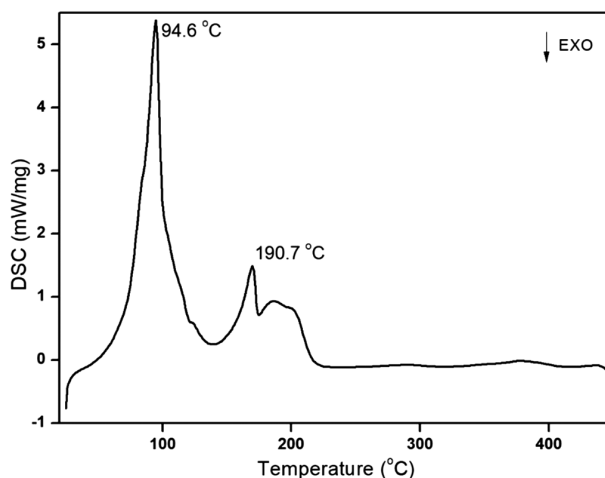
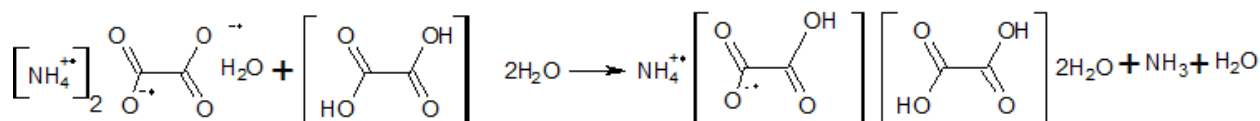


Fig. 1 — DSC curve for ATOXAL.

Table 1 — Crystallographic data of ATOXAL single crystal.

Lattice parameters	Present work	Reported value
a (Å)	6.349	6.3387
b (Å)	7.246	7.227
c (Å)	10.58	10.5527
α	94.17	94.172
β	100.12	100.274
γ	97.86	97.704
Volume (Å ³)	472.3	468.77



Scheme 1 — Reaction mechanism

anomalies in the dielectric, elastic and thermal properties of the material. These generally occur when such materials undergo a structural phase transition from a high temperature paraelectric phase to a low temperature ferroelectric phase. The results due to the dielectric anomaly is dealt with as follows.

3.2.1 Variation of dielectric parameters with frequency

The dielectric constant was calculated using:

$$\epsilon' = \frac{Cd}{\epsilon_0 A} \quad \dots (1)$$

where C is the capacitance, d is the thickness, A is the area and ϵ_0 is the absolute permittivity of free space.

ϵ'' is the imaginary dielectric constant calculated using the relation

$$\epsilon'' = \epsilon' \tan \delta \quad \dots (2)$$

where $\tan \delta$ is the dielectric loss. From Fig. 2, the variation of the dielectric constant with frequency, it is observed that there is a decrease of the dielectric constant with an increase in frequency, due to the presence of all polarisations at low frequencies and the loss of these at high frequencies. At low frequencies, the purity and perfection of the crystal is noticed due to the domination of the space charge polarisation. This space charge polarisation arises due to charged lattice defects¹⁰. A similar but gradual decrease is seen in the variation of the imaginary dielectric constant and dielectric loss with frequency, which suggests that different domain sizes have varied relaxation times. Stray capacitances resulted in the variation of space charge polarisation in the high frequency region.

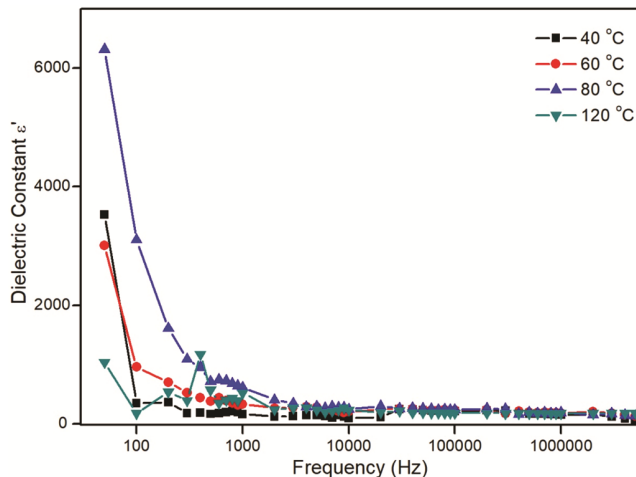


Fig. 2 — Variation of dielectric constant ϵ' with frequency.

The weak frequency dependence of dielectric loss accompanied by a decrease at higher frequencies, is suitably explained by the dielectric modulus M which is used to analyze ionic conductivities. The dielectric modulus corresponds to the relaxation of the electric field in the material when the electric displacement remains a constant¹¹. The dielectric modulus is defined by:

$$M = (\epsilon^*)^{-1} \quad \dots (3)$$

where $\epsilon^* = \epsilon' - i\epsilon''$ is the complex dielectric constant; ϵ' and ϵ'' are the real and imaginary parts of the dielectric constant. The imaginary part of dielectric modulus is given by:

$$M'' = \frac{\epsilon''}{\epsilon'^2 + \epsilon''^2} \quad \dots (4)$$

Figure 3 shows the imaginary part of the dielectric modulus M'' in the frequency range from 100 Hz to 1 MHz at various temperatures. It is noticed that peaks are observed in dielectric modulus spectra. The peak shifts to higher frequency at the phase transition temperature of 100 °C. The low frequency side of peak represents the range of frequencies in which the ions can move over long distances, i.e., ions can perform successful hopping from one site to the neighbouring site. Whereas, for the high frequency side, the charges are not able to respond to alternating electric field and they can only execute localized motion¹².

A similar explanation will suffice the variation of capacitance, a function of dielectric constant ϵ' with frequency. The mean carrier hopping on defects leads to rapid redistribution of charges on the defects at low

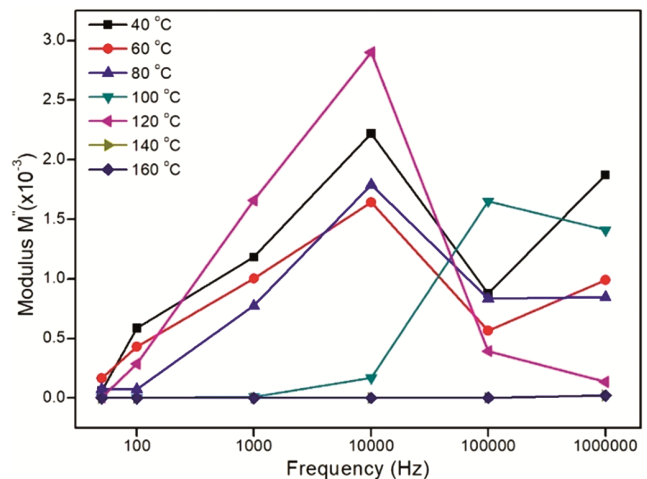


Fig. 3 — Dielectric modulus spectra for various temperatures.

frequencies. Whereas at high frequencies, a decrease in capacitance is due to lack of time to redistribute the charges in accordance to the applied voltage^{13,14}.

3.2.2 Variation of dielectric parameters with temperature

Figure 4 shows the variation of dielectric constant as a function of temperature. A complicated manipulation of the dielectric constant by the temperature is seen in the temperature range from 40 °C – 160 °C in ATOXAL crystal. The dielectric constant peaked up at 100 °C and 140 °C revealing that there are two phase transitions and are nearly in accordance to that seen in the DSC curve in Fig. 1. The minor difference in values could be due to the different heating rates of the sample during both the thermal and dielectric studies. The first ε' peak may be due to the dissociation of the water molecules resulting in the switching of the dipoles formed by the oxygen vacancies (positively charged) with the acceptor hydroxyl ions (negatively charged) and the second ε' peak may be due to the structural changes in the oxalate ion⁷ leading to space charge accumulation¹⁵ at high temperatures. Oxygen vacancies are the most important point defects in ferroelectric materials. These double peaks give rise to a characteristic pinched P-E loop¹⁶.

The temperature dependence of 1/ε' for various frequencies is also an evidence for the existence of relaxor behaviour in ferroelectrics. Figure 5 shows the variation of 1/ε' as a function of temperature at 1 kHz. From this plot three temperature regions namely, T_m, the ferroelectric transition temperature; T_C, the Curie temperature and T_{CW}, the Curie-Weiss temperature can be determined. The extrapolation of the linear

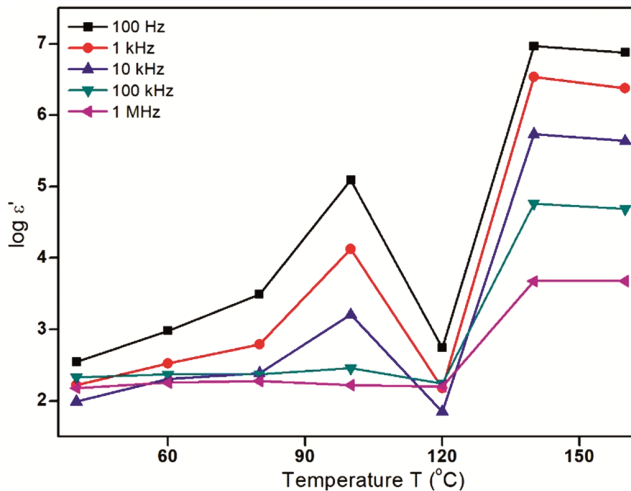


Fig. 4 — Variation of dielectric constant ε' with temperature T.

behaviour T_{CW} on the temperature axis is used to determine the apparent Curie temperature¹⁷ T_C. Above T_m, a strong deviation from classical Curie-Weiss law 1/ε' ∝ T⁻¹ is observed in all relaxor ferroelectric materials. This deviation can be described by the quadratic power law 1/ε' ∝ (T - T_m)². The values of T_C, T_m and T_{CW} for various frequencies are listed in Table 2.

The diffuseness of the relaxor ferroelectrics can be further explained by fitting the dielectric data with the modified Curie-Weiss law. The power function relation is used to evaluate the degree of dielectric relaxor properties in a quantitative way¹⁸.

$$\frac{1}{\epsilon'} - \frac{1}{\epsilon'_{\max}} = \frac{(T - T_{C_{\max}})^\gamma}{C} \quad \dots (5)$$

where ε'_{max} is dielectric maximum at T_C; C is a material related constant; T_{Cmax} stands for the absolute temperature at dielectric maximum, and γ is the relaxation factor standing for the degree of diffuseness of phase transition, with values ranging from 1 to 2 and the ferroelectric nature varying from a normal one to that of a relaxor. The diffusivity γ corresponds to a very broad relaxation and higher

Table 2 — T_m, T_C and T_{CW} for various frequencies of ATOXAL.

Temperature	Frequency			
	100 Hz	1 kHz	10 kHz	100 kHz
T _m	368	369.4	370	370.4
T _C	369.8	371.2	371	351.6
T _{CW}	375.2	376	373.8	376.5

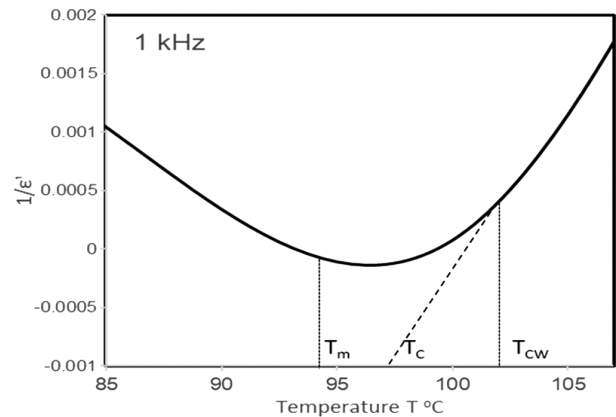


Fig. 5 — Variation of $\frac{1}{\epsilon'}$ with temperature T at 1 kHz for the determination of T_m, T_C and T_{CW}.

disorder. The diffusivity curve given in Fig. 6 is plotted with the data obtained at 1 kHz and the slope of the fitting line is 1.177, suggesting that ATOXAL single crystal stays at an intermediate state between normal and relaxor ferroelectric.

Good optical quality crystals with few defects showed low dielectric losses with high frequency¹⁹. The dielectric loss increases with temperature and is presented in the plot of $\tan \delta$ versus temperature shown in Fig. 7. The dielectric loss behaviour with temperature is typical of polar dielectrics where losses occurred due to electrical conduction apart from dipole losses²⁰. Also, domain wall motion accompanied by domain shape change and mobility is the primary reason for the dielectric loss in the ferroelectric phase, very close to T_C . Hence, there

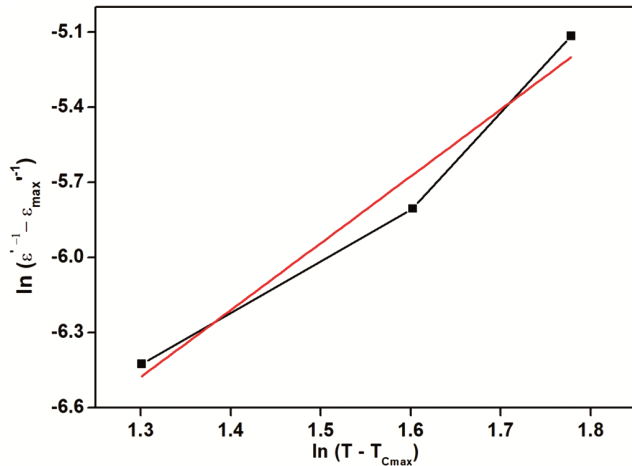


Fig. 6 — Plot of $\ln \frac{1}{\epsilon'} - \frac{1}{\epsilon'_{\max}}$ and $\ln(T - T_{C\max})$.

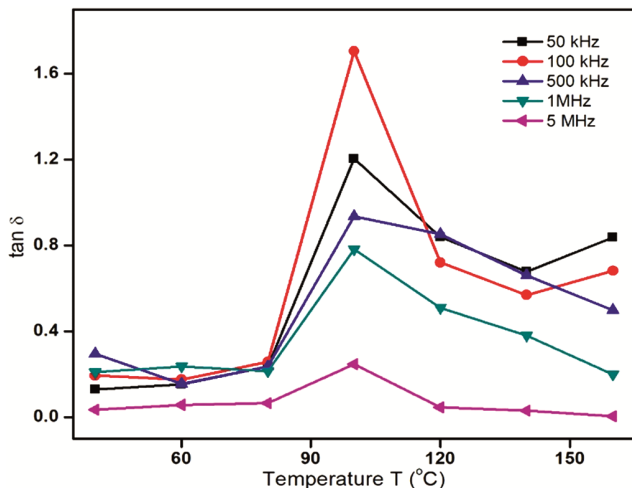


Fig. 7 — Variation of $\tan \delta$ with temperature T .

exists the prominence of polarization switching within domains in the vicinity of T_C .

The AC electrical conductivity σ is calculated using the dielectric data using the relation

$$\sigma = \omega \epsilon' \epsilon_0 \tan \delta \quad \dots (6)$$

where ϵ_0 is the permittivity of free space and ω is the angular frequency. The AC conductivity σ follows a similar pattern as that of ϵ' , with anomalies at 100 °C and 140 °C and decreasing thereafter. The large increase in the mobile charge carrier (H^+ and OH^- ions) concentration and defects in this region is the reason for the rapid increase in conductivity²¹. Thus, the movement of intrinsic defects produced due to thermal fluctuations and whose concentration increases exponentially with temperature are the causes for the increase in conductivity in the higher temperature region.

The Arrhenius equation,

$$\sigma = \sigma_0 \exp\left(\frac{-E_a}{kT}\right) \quad \dots (7)$$

is used to calculate the activation energy E_a before and after the phase transition. The activation energies for selected frequencies is listed in Table 3 and the variation of the activation energy with frequency is shown in Fig. 8. A change in slope is seen exactly at

Table 3 — Activation energies for various frequencies of ATOXAL.

Frequency (Hz)	E_a (eV)
100	1.674
200	1.7
800	1.740
900	1.762
1000	1.772

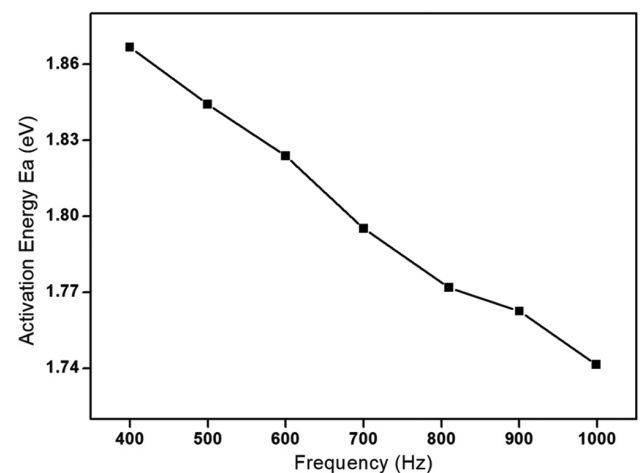


Fig. 8 — Variation of activation energy E_a with frequency.

the material's phase transition temperature which is the characteristic of ferroelectric materials²².

The ferroelectric and paraelectric phases differ in their activation energies due to the grain boundary effect. Also, charge carriers require large activation energy to move from the ordered state in the ferroelectric phase to the disordered state in the paraelectric phase. The activation energies in the ferroelectric (E_F) and paraelectric (E_P) phases were found to be 1.772 eV and 3.476 eV, respectively, at a frequency of 1 kHz. Higher activation energy is required by the charge carriers to jump across adjoining sites in the paraelectric phase. Proton transfer through hydrogen bonds enabled electrical conductivity suggesting that ATOXAL is a protonic conductor.

3.2.3 Variation of other dielectric parameters with frequency and temperature

AC conductivity and its variation with frequency is a well-established method to characterize the hopping dynamics of the charge carriers / ions. The frequency dependence of AC conductivity σ at various temperatures in Fig. 9 shows that at low frequencies and high temperatures, plateaus of σ (i.e., frequency independent values of conductivity) which correspond to the DC conductivity are seen. The observed frequency dependent conductivity obeys Jonscher's universal power law given by:

$$\sigma(\omega) = \sigma_0 + A\omega^n \quad \dots (8)$$

where $\omega = 2\pi f$. The slope of $\ln \sigma$ with $\ln \omega$ gives the value of the frequency dependent exponent n and represents the many body interactions of electrons,

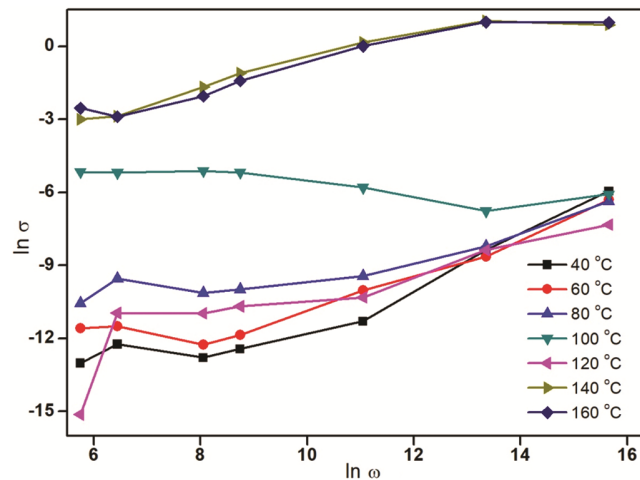


Fig. 9 — Variation of $\ln \sigma$ with $\ln \omega$.

charges and impurities²³. The variation of $\ln \sigma$ with $\ln \omega$ at 80 °C presented in Fig. 10 shows two threshold frequencies f_1 and f_2 , separating the entire variation into three regions: (i) low frequency region, $f < f_1$; in which the conductivity is almost frequency-independent and called σ_{DC} . (ii) moderate frequency region, $f_1 < f < f_2$; and (iii) high frequency region, $f > f_2$ is where the conductivity increases linearly with the frequency. The value of n was obtained by fitting $\ln \sigma$ versus $\ln \omega$ plots in the moderate frequency region. It depends on the temperature of the sample and for ideal Debye samples, $n = 1$ and for others²⁴, $n \leq 1$. In the current region of interest, the value of n for ATOXAL crystal was found to be 0.5, i. e., $0 < n < 1$. This reveals that the conduction mechanism in this region corresponds to the translational hopping motion^{25,26}. This hopping motion of the charge carriers is short range and occurs through energy barrier separated traps²³. In high frequency region, the n value is nearly 1, i. e. $1 < n < 2$, which reveals that the conduction mechanism in this range of frequency corresponds to the well-localized hopping and/or reorientational motion^{25,26}.

The frequency exponents for various temperatures are estimated from the slopes of $\ln \sigma$ versus $\ln \omega$ plots. The exponent decreases with temperature till the phase transition temperature and later increases as seen in the inset of Fig. 10 which is the variation of frequency exponent n with temperature. It is therefore inferred that the many body interactions are least at the phase transition temperature and higher at other temperatures.

When the temperature is in the vicinity of the Curie point T_C , the ferroelectric materials show

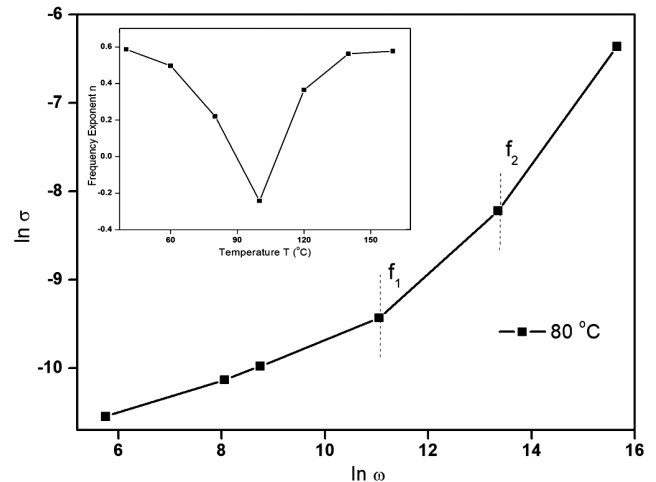


Fig. 10 — Determination of threshold frequencies at 80 °C; (inset) variation of frequency exponent n with temperature.

incongruities in the dielectric, elastic, thermal and other thermodynamic properties and the dielectric constant in most ferroelectric crystals has an abnormally large value (up to $10^4 \sim 10^5$) near²⁷ T_C . This phenomenon is usually called “dielectric anomaly” and considered to be the basic feature of ferroelectric materials.

Above the transition temperature the electrical susceptibility χ , of the substance follows the law:

$$\chi = \frac{A}{T - T_C} \quad \dots (9)$$

where A is a constant. This is in the same form of the Curie–Weiss law of magnetic susceptibility. For ferroelectrics, the above expression is no more than a mean-field approximation applied to the fluctuating local electric fields in the crystal structure. Figure 11 shows the temperature dependent variation of susceptibility.

A simple method of determining electrical susceptibility is to measure the capacitance of a parallel plate capacitor containing the ferroelectric substance as a dielectric. Capacitance C , is related to susceptibility through the expression:

$$C = C_0(1 + \chi) \quad \dots (10)$$

where C_0 is the capacitance without a dielectric and is determined from:

$$C_0 = \frac{\epsilon_0 A}{d} \quad \dots (11)$$

where A is the area of the capacitor plate, d is the distance between the plates and $\epsilon_0 = 8.85 \times 10^{-12} \text{ Fm}^{-1}$.

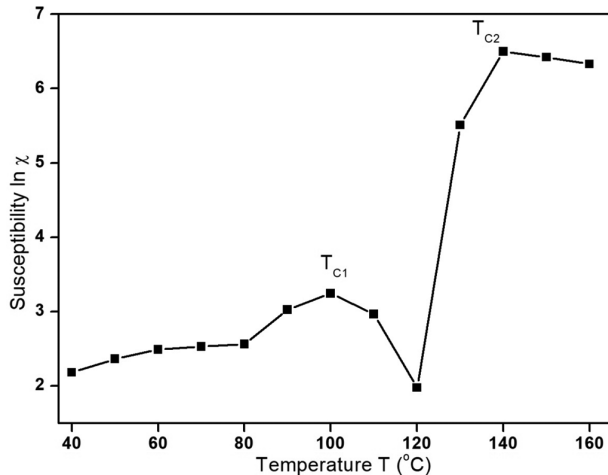


Fig. 11 — Variation of susceptibility χ with temperature T .

3.3 Penn gap analysis

The internal consistency between the phenomenological approach of Clausius-Mossotti and the band structural approach of Penn was proved from the following.

The valence electron plasma energy $\hbar\omega_p$ was calculated from²⁸:

$$\hbar\omega_p = 28.8 \sqrt{\frac{Z\rho}{M}} \text{ eV} \quad \dots (12)$$

where Z is the number of valence electrons, ρ is the density and M is the molecular weight.

The Penn gap E_p and E_f are solely dependent on the plasma energy $\hbar\omega_p$ and are given by²⁹:

$$E_p = \frac{\hbar\omega_p}{(\epsilon_\infty - 1)^{1/2}} \quad \dots (13)$$

and

$$E_f = 0.2948 (\hbar\omega_p)^{4/3} \quad \dots (14)$$

The electronic polarisability α is a function of E_p and was obtained using the relation³⁰:

$$\alpha = \frac{(\hbar\omega_p)^2 S_0}{(\hbar\omega_p)^2 S_0 + 3E_p^2} \times \frac{M}{\rho} \times 0.396 \times 10^{-24} \quad \dots (15)$$

where S_0 is a constant and is given by:

$$S_0 = 1 - \frac{E_p}{4E_f} + \frac{1}{3} \left(\frac{E_p}{4E_f} \right)^2 \quad \dots (16)$$

The value of the electronic polarisability α obtained through the phenomenological approach, the Clausius–Mossotti relation is given by:

$$\left(\frac{\epsilon_\infty - 1}{\epsilon_\infty + 2} \right) \times \frac{M}{\rho} = 2.53 \times 10^{24} \alpha \quad \dots (17)$$

$$\alpha = \frac{3M}{4\pi N_a \rho} \left(\frac{\epsilon_\infty - 1}{\epsilon_\infty + 2} \right) \quad \dots (18)$$

where N_a is the Avogadro number.

The calculated data for the grown crystal are tabulated in Table 4. The consistency in the approaches of Penn and Clausius - Mossotti are revealed in the above analysis.

3.4 Piezoelectric (d_{33}) measurement

A piezoelectric substance is one that produces an electric charge when a mechanical stress is applied. The ATOXAL crystal sample was poled at room temperature by immersing it in silicon oil and applying a dc poling field of 20 kVcm^{-1} for 20 min. Confirmation of piezoelectric properties was done by determining the coupling or piezoelectric charge coefficient ($d_{33} \text{ pCN}^{-1}$) on applying a tapping force of 0.25 N at a tapping frequency of 110 Hz. Piezoelectric d_{33} coefficient was determined using the relation:

$$d_{33} = \frac{Q/A}{F/A} = \frac{Q}{F} \text{ CN}^{-1} = \frac{CV}{F} \quad \dots (19)$$

Table 4 — Penn Analysis for ATOXAL.

Plasma energy (eV)	23.162	
Penn gap (eV)	1.892	
Fermi energy (eV)	19.464	
Polarisability (cm^3)	Penn	Clausius-Mossotti
	5.5195×10^{-23}	5.5301×10^{-23}

where A is the area on which a force F is applied, C is the capacitance in the circuit and V is the voltage generated. The d_{33} value is found to be 1.5 pCN^{-1} for the grown crystal.

3.5 P-E loop trace

Well-defined hysteresis loops were traced at a frequency of 50 Hz. The unpoled crystal exhibited randomly distributed spontaneous polarization in different orientation states. This is due to the cancellation of the piezoelectric effect in different regions and the net piezoelectric effect becomes weaker. Figure 12 shows the room temperature hysteresis loops traced for the poled as grown ATOXAL crystal. It is seen that the loops are perfect, indicative of good quality and strain free single crystals. The value of remnant polarization (P_r), saturation polarisation (P_s) and coercive field (E_c) are $\sim 0.367 \mu\text{C/cm}^2$, $\sim 1.789 \mu\text{C/cm}^2$ and $\sim 6.599 \text{ kV/cm}$, respectively, for the grown sample. In the present investigation, elliptical shaped loops were obtained

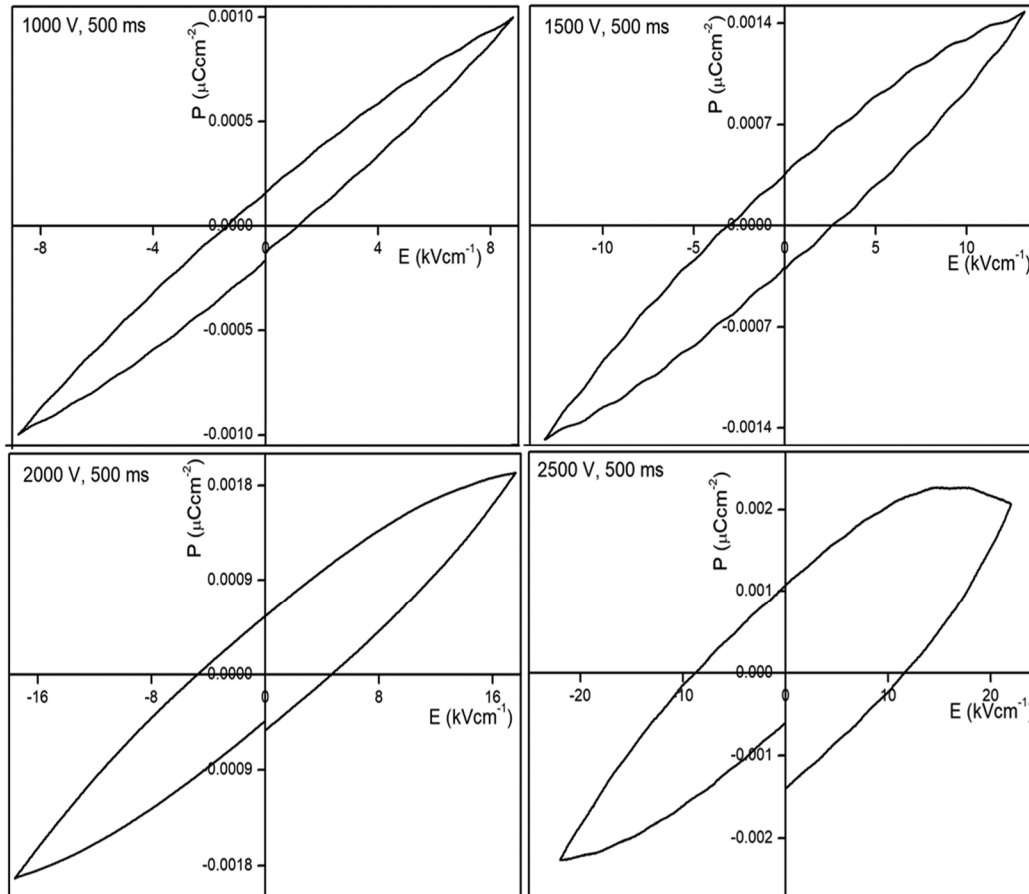


Fig. 12 — P - E hysteresis loops for the poled ATOXAL crystal.

indicating the good ferroelectric nature of the ATOXAL crystal. An increase in the applied electric field increases the area of the hysteresis curve, i.e., retentivity and coercivity increase. A ferroelectric materials' hysteresis curve is evaluated by the squareness of the hysteresis loop given by³¹:

$$R_{sq} = \frac{P_r}{P_s} + \frac{P_{1.1E_c}}{P_r} \quad \dots (20)$$

where R_{sq} and $P_{1.1 E_c}$ represents squareness of the P-E loop and the polarization under the external field of 1.1 E_c , respectively. The R_{sq} value was determined to be 0.32 while ideal hysteresis loops possess the R_{sq} value of 2. The shapes of the loops depend strongly on the nature of the material as well as the applied electric field during poling.

4 Conclusions

In conclusion, ATOXAL single crystal grown by slow evaporation technique possessed fairly good dielectric, ferroelectric and piezoelectric properties suitable for device application. From the various dielectric measurements, it was observed that anomalies occurred at the phase transition temperature of 100 °C. The activation energies before and after the phase transition were found to be different. The frequency exponent was at its least at the phase transition temperature. The ferroelectric susceptibility curve also established that phase transition occurred at the said temperature. The diffuseness degree of the phase transition for the unpoled single crystal was calculated to be 1.177, implying the sample was at an intermediate state between normal and relaxor ferroelectrics. A low piezoelectric coefficient d_{33} value obtained. Tensile stresses may have opposed the poling induced orientation of domains. The area of the hysteresis loops before and after poling differed.

Acknowledgment

The authors express their heartfelt gratitude for the technical support rendered by Dr Binay Kumar and his research team at the University of Delhi.

References

- 1 Hooton J A & Merz W J, *Phys Rev*, 98 (1955) 409.
- 2 Arlt G & Sasko P, *J Appl Phys*, 51 (1980) 4956.
- 3 Currie M & Speakman J C, *J Chem Soc*, (1967) 1862.

- 4 Biyik R, Taparmaz & Karabulut B, *Z Naturforsch*, 58A (2003) 499.
- 5 Marcello C & Gustavo P, *Acta Cryst E*, 62 (2006) 4725.
- 6 Marmier A, Lethbridge Z A D, Walton R I, Smith C W, Parker S C & Evans K E, *Comp Phys Comm*, 181 (2010) 2105.
- 7 Eunice J, Infant S K M, Shahil K S & Gopala K R, *Optik*, 127 (2016) 3896.
- 8 Shakir M, Singh B K, Kumar B & Bhagavannarayana G, *Appl Phys Lett*, 95 (2009) 252902.
- 9 Chen Q, Li X, Zhang Y & Qian Y, *Adv Mater*, 14 (2002) 134.
- 10 Arora S K, Patel V, Amin B & Kothari A, *Bull Mater Sci*, 27 (2004) 141.
- 11 Yi Z, Juan A & Guang-Lin Z, *Open J Org Pol Mater*, 3 (2013) 99.
- 12 Liu J J, Duan C G, Yin W G, Mei W N, Smith R W & Hardy J R, *J Chem Phys*, 119 (2003) 2812.
- 13 Zukowski, Kantorov S B, Maczka D & Stelmakh V F, *Phys Status Solidi A*, 112 (1989) 695.
- 14 Vasudevan A, Carin S, Melloch M R & Hannon E S, *Appl Phys Lett*, 73 (1998) 671.
- 15 Vonhippel A, *Materials and Applications*, New York, (1965) 79.
- 16 Yan H, Inam F, Viola G, Ning H, Zhang H, Jiang Q, Zeng T A O, Gao Z & Reece M J, *J Adv Dielect*, 1 (2011) 107.
- 17 Pelaiz-Barranco A, Gonzalez-Carmenate I & Calderon-Pinar F, *Solid State Commun*, 134 (2005) 519.
- 18 Chen J, Fan H, Ke S, Chen X, Yang C & Fang P, *J Alloys Compd*, 478 (2009) 853.
- 19 Madhavan J, Aruna S, Prabha K, Julius J P, Joseph G P, Selvakumar S & Sagayaraj P, *J Cryst Growth*, 293 (2006) 409.
- 20 Kumar A, Raju K J & James A R, *J Mater Sci: Mater Elect*, 28 (2017) 13928.
- 21 Jain S C & Dahake S L, *Indian J Pure Appl Phys*, 2 (1964) 71.
- 22 Choudhary R N P, S R Shannigrahi & Singh A K, *Bull Mater Sci*, 22 (1999) 975.
- 23 Angadi B, Victor P, Jali V M, Lagare M T, Kumar R & Krupanidhi S B, *Mater Sci Eng B*, 100 (2003) 93.
- 24 Gudmundsson J T, Svavarsson H G, Gudjonsson S & Gislason H P, *Phys B: Cond Matter*, 340 (2003) 324.
- 25 Ram M & Chakrabarti S, *J Alloys Compd*, 462 (2008) 214.
- 26 Akgul U, Ergin Z, Sekerci M & Atici Y, *Vacuum*, 82 (2008) 340.
- 27 Yuhuan X, *Ferroelectric materials and their applications*, (North-Holland), 1991.
- 28 Jackson J D, *Classical electrodynamics*, (Wiley Eastern: New York), 1978.
- 29 Ravindra N M, Bharadwaj R P, Sunil Kumar & Srivastava V K, *Infrared Phys*, 21 (1981) 369.
- 30 Ravindra N M & Srivastava V K, *Infrared Phys*, 20 (1980) 67.
- 31 Hou Y D, Wu N N, Wang C, Zhu M K & Song X M, *J Am Ceram Soc*, 93 (2010) 2748.